

INTERNATIONAL SOCIETY FOR SOIL MECHANICS AND GEOTECHNICAL ENGINEERING



This paper was downloaded from the Online Library of the International Society for Soil Mechanics and Geotechnical Engineering (ISSMGE). The library is available here:

<https://www.issmge.org/publications/online-library>

This is an open-access database that archives thousands of papers published under the Auspices of the ISSMGE and maintained by the Innovation and Development Committee of ISSMGE.

Deformation property of shear band in sand subjected to plane strain compression and its relation to particle characteristics

Relations caractéristiques entre la déformation des bandes de cisaillement dans les sables soumis à la compression en déformation plane et les particules des sables

Teru Yoshida – *Kajima Technical Research Institute, Tokyo, Japan*
 Fumio Tatsuoka – *Department of Civil Engineering, University of Tokyo, Japan*

ABSTRACT: The deformation characteristics of shear band in sands, gravels and glass ballotini during plane strain compression (PSC) were investigated, and they were linked with particle size, crushability and shape. It is shown that the deformation characteristics of shear band is controlled primarily by particle size, and secondarily by particle crushability, relating to the pressure level at each PSC test. Effect of particle shape is less significant.

RESUME: Les caractéristiques de la déformation des bandes de cisaillement dans les sables, les graviers et les billes de verre soumis à la compression en déformation plane ont été étudiées, et elles ont été reliées à la taille moyenne, l'aptitude à s'écraser et la forme des grains. On montre que les caractéristiques de la déformation des bandes de cisaillement dépendent essentiellement de la taille des grains, et secondairement de l'aptitude à s'écraser des grains, en relation avec le niveau de la pression à chaque essais de déformation plane. L'effet de la forme des grains est moins significatif.

1 INTRODUCTION

The failure of a soil mass in a boundary value problem is usually progressive in the sense that the peak-strength is not mobilized simultaneously along the whole of potential slip surface (shear band) at any instance. The shear deformation and dilatancy characteristics of shear band in soil during the post-peak strain softening regime are, therefore, essential for any rational numerical analyses of the failure of soil. In parallel to the above, in an element test such as plane strain compression (PSC) test, in the post-peak regime, strains averaged for a whole specimen are subjective depending on the specimen size, because each shear band has a characteristic thickness which may be inherent to each material under given stress conditions. On the other hand, the deformation characteristics of shear band can be considered to be

essentially objective, and should be incorporated in the failure analyses of a soil mass.

To investigate the deformation characteristics of shear band and their relation to size, crushability and shape of particles, we performed a series of PSC tests using 12 kinds of poorly graded granular materials listed in Table 1 (see also Fig. 1).

2 PLANE STRAIN COMPRESSION (PSC) TESTS

Test specimens were 57, 24 and 21 cm in the directions of σ_1 , σ_2 and σ_3 (large-size) for Hime and Isomi gravels or 20, 16 and 8 cm (medium-size) for the other materials. Dense specimens were prepared by pluviating air-dried particles through air with the direction of pouring coinciding with the direction of σ_1 and were kept air-dried throughout each test.

The lateral surface of the specimen was covered with a latex rubber membrane having a thickness of either 0.8 or 2.0 mm (large-size) or 0.3 mm (medium-size). The surfaces of σ_1 and σ_2 were well lubricated. One of the two confining platens, in contact with the σ_2 surfaces, was made of transparent Acryle to observe the deformation of specimen. The details of the medium-size apparatus and the testing method are given in Goto et al. (1993) and Tatsuoka et al. (1994). The mechanical configuration and testing method for the large-size apparatus were similar to those for the medium-size one.

Table 1. List of test materials.

Material (Origin)	D_{50} mm	U_c	G_s	e_{max}	e_{min}	Grain shape
Ottawa sand (USA)	0.174	1.76	2.67	0.864	0.515	Sub-rounded
Wakasa sand (Japan)	0.197	1.72	2.72	1.223	0.787	Sub-angular
Toyoura sand (Japan)	0.206	1.58	2.64	0.973	0.612	Sub-angular
Hostun sand (France)	0.408	2.13	2.64	0.95	0.55	Sub-angular
Karlsruhe sand (Germany)	0.460	1.61	2.65	0.87	0.54	Intermediate
Monterey sand (USA)	0.484	1.40	2.64	0.86	0.55	Intermediate
Glass ballotini (Japan)	0.499	1.20	2.49	0.713	0.563	Sphere
Ticino sand (Italy)	0.527	1.52	2.68	0.96	0.59	Sub-angular
Silver Leighton Buzzard (S.L.B.) sand (UK)	0.681	1.43	2.66	0.79	0.49	Intermediate
Hasaki sand (Japan)	1.62	1.36	2.65	0.884	0.700	Sub-angular
Hime gravel (Japan)	2.01	1.40	2.65	0.633	0.514	Sub-rounded
Isomi gravel (Japan) ¹⁾	6.80	1.46	2.67	-	-	Sub-rounded

¹⁾ e_{max} and e_{min} could not be measured.

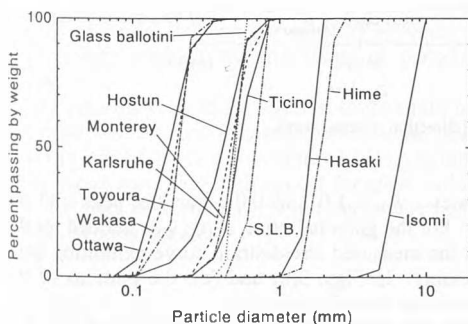


Figure 1. Grain size distribution curves of the test materials.

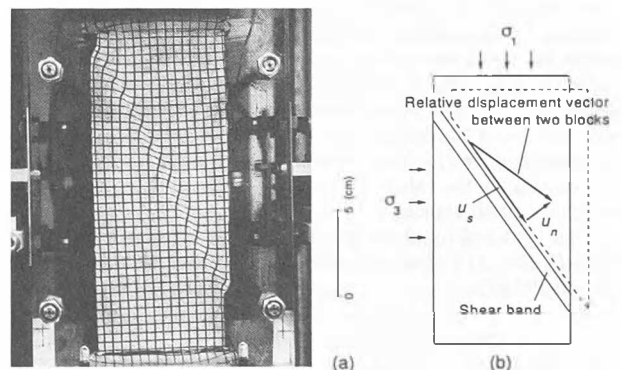


Figure 2. (a) Typical test (Ticino sand, $\sigma_3 = 78$ kPa, $\gamma = 13.3\%$), (b) Definition of u_s and u_n .

Table 2. List of PSC tests.

Material ¹⁾	σ_3 kPa	D_r ²⁾ %	ϕ_{peak} deg	ν_f deg	ϕ_{res} deg	θ deg	t_0 mm	γ_{peak} ³⁾ %	$(u_s)_{res}$ mm
Ottawa	78	75	43.4	21.4	34.0	70	3.7	4.1	2.10
	392	73	44.3	15.0	32.2	65	3.6	6.4	2.04
Wakasa	78	144	55.5	31.2	41.7	64	4.3	6.7	1.77
Toyoura	78	76	45.3	25.7	36.9	66	3.5	4.8	2.24
	196	86	45.9	22.8	35.0	65	3.1	5.5	2.65
392	85	45.0	19.5	33.7	66	2.5	7.4	2.51	
	78	82	47.6	23.8	35.9	63	6.2	6.0	3.36
392	74	44.8	17.6	34.2	58	2.8	9.5	2.02	
	78	72	43.8	21.7	33.0	59	4.5	7.1	3.64
392	68	42.8	21.7	31.0	58	4.2	8.9	4.04	
	78	79	47.7	27.4	34.4	66	5.3	4.6	3.69
392	67	45.5	18.0	34.7	59	3.6	7.7	2.56	
	78	85	35.7	19.1	26.5	54	9.8	4.0	5.03
392	53	32.3	14.6	26.2	53	9.0	5.8	8.29	
	78	79	48.1	25.1	34.8	61	5.1	7.2	4.62
392	73	45.7	21.2	34.5	60	3.6	11.1	3.06	
	78	75	44.7	25.6	32.7	59	6.1	7.4	4.50
196	75	43.4	25.7	31.3	62	5.8	6.9	5.90	
	392	76	42.5	22.4	30.8	61	5.5	7.6	4.57
Hasaki ⁴⁾	392	127	44.3	23.6	33.7	53	7.1	9.5	6.66
392	126	44.5	18.3	35.3	56	8.4	8.7	7.81	
	78	80	48.1	12.4	36.5	60	15.8	4.9	12.1
78	83	48.7	13.2	37.4	62	14.6	5.0	11.3	
	78	87	48.6	12.1	37.0	61	14.7	5.0	12.5
Hime ⁵⁾	78	89	49.9	21.3	40.2	60	21.2	4.5	9.41
Hime ⁶⁾	78	-	54.7	19.8	46.1	56	23.8	9.9	12.6

1) Except for Hime gravel and Isomi gravel, 0.3 mm-thick membrane was used.

2) Relative density at the start of PSC loading.

3) Average shear strain at peak stress state.

4) Average of two tests is plotted in Figs. 5 and 8.

5) Membrane thickness was 0.8 mm. Average of these three test results is plotted in Figs. 5 and 8.

6) Tests were performed by Dr. J. Dong of Tokyu Construction Co., Ltd. and pictures were provided. The membrane thickness was 2.0 mm. These data were excluded when regression curves in Fig. 5 were calculated.

A constant rate of axial strain of 0.0625 %/min (large-size) or 0.125 %/min (medium-size) was applied while σ_3 was kept constant, equal to 78 kPa (0.8 kgf/cm²), 196 kPa (2.0 kgf/cm²) or 392 kPa (4.0 kgf/cm²). For the tests at $\sigma_3 = 196$ and 392 kPa, air confining pressure was applied in the combination with partial vacuum of 78 kPa applied to the inside of specimen.

Grids made of dyed latex rubber had been printed in advance on the outer surface of the latex rubber membrane on the σ_2 surface (Fig. 2a). Many pictures of the σ_2 surfaces were taken through the transparent confining platen during each test. In the tests at $\sigma_3 = 196$ and 392 kPa, pictures were taken from outside of the transparent pressure cell, and the distortion of pictures was properly corrected. The coordinates of the nodes of grids on each picture were read automatically to an accuracy of 0.03 mm or better by means of a photogrametric system.

3 PROPERTIES OF SHEAR BAND OBSERVED IN PSC TESTS

Part of the test results are listed in Table 2. The shear deformation of a shear band u_s and the increase in the shear band thickness u_n (Fig. 2b) were obtained by integrating the increments of u_s and u_n observed between two successive loading stages. The values of u_s and u_n were obtained in such that components due to homogeneous deformation of the specimen were not included in these values (Yoshida et al., 1994). These quantities were obtained from the changes in the coordinates of nodes located immediately outside the boundaries of the finally appeared single shear band. In so doing, only central part of shear band for about 50 to 70 % of the full width of the specimen was used. The deformation in the post-peak regime was obtained as $u_s' = u_s - (u_s)_{peak}$ and $u_n' = u_n - (u_n)_{peak}$, where $(u_s)_{peak}$ and $(u_n)_{peak}$ are the values of u_s and u_n observed at the peak state, which are small values.

Figs. 3(a) and (c) show the relationships between shear stress level R_n (Eq. 1) and shear deformation of shear band u_s' at $\sigma_3 = 78$ and 392 kPa:

$$R_n = \frac{(\sigma_1 / \sigma_3) - (\sigma_1 / \sigma_3)_{res}}{(\sigma_1 / \sigma_3)_{peak} - (\sigma_1 / \sigma_3)_{res}} \quad (1)$$

where $(\sigma_1 / \sigma_3)_{peak}$ and $(\sigma_1 / \sigma_3)_{res}$ are the σ_1 / σ_3 ratios at the peak

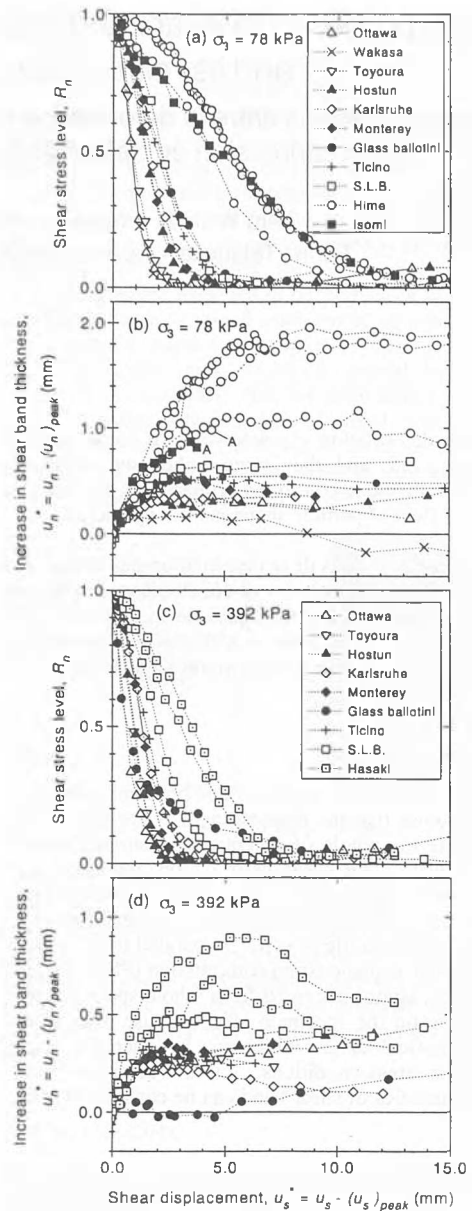


Figure 3. Observed deformation in shear band.

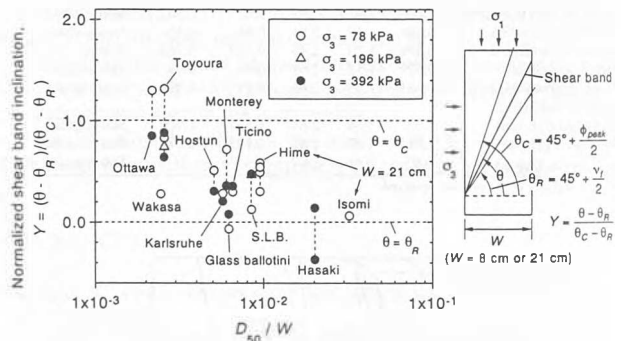


Figure 4. Observed direction of shear band.

and residual states. $R_n = 1.0$ and 0.0 mean the peak and the residual states. For the glass ballotini, σ_1 / σ_3 was defined for the top envelope of the measured stress-strain curve exhibiting large stick-slip behaviour. In Figs. 3(a) and (c), the patterns of the curves are very similar to each other.

Figs. 3(b) and (d) show the relationships between u_n' and dilatation u_n' . Comparing Fig. 3(b) with Fig. 3(a) and Fig. 3(d)

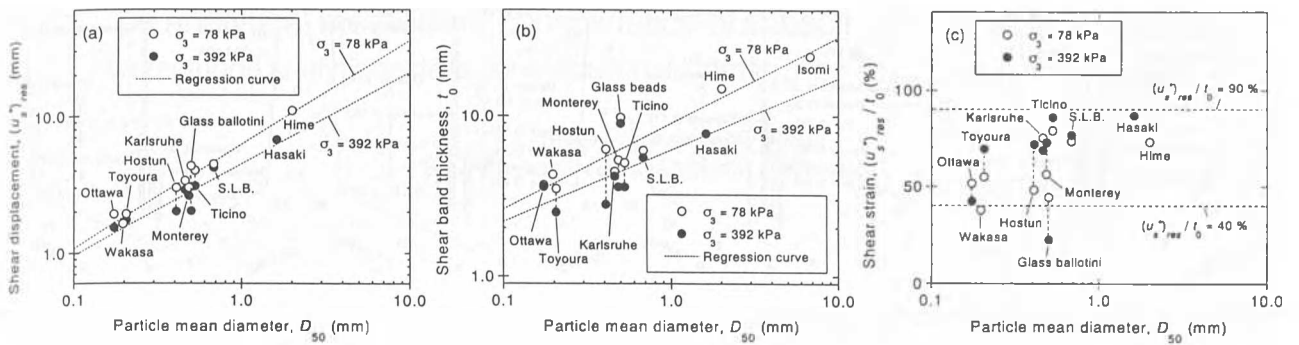


Figure 5. Influence of particle diameter D_{50} on $(u_s^*)_{res}$ and t_0 .

with Fig. 3(c), it is seen that in each test, the largest rate of dilatation is attained near the peak state, and then the rate of dilatation decreases gradually to zero before the start of residual state (Yoshida et al., 1994). For the two large-size PSC tests using a 2.0 mm-thick membrane, u_s^* and u_n^* relations after u_s^* exceeded about 4 mm exhibited largely decreasing rates of u_n^* . This peculiar behaviour was considered due to the effects of membrane force exerting to largely straining shear bands. Therefore, in Fig. 3(b), plots were terminated at the points denoted by the letter A. Some decrease in u_n^* in the post-peak regime seen in Fig. 3(d) would be due to another mechanism. From these figures, it is seen that the values of u_s^* and u_n^* at the start of residual state increase with particle size.

The average angle θ of the orientation of shear band relative to the σ_3 direction measured at the start of the residual state are listed in Table 2. In Fig. 4, the normalized shear band direction $Y = (\theta - \theta_R)/(\theta_C - \theta_R)$ is plotted against the ratio of the mean particle diameter D_{50} to the specimen width W : where $\theta_C = 45^\circ + \phi_{peak}/2$ (direction of maximum stress obliquity) and $\theta_R = 45^\circ + \nu_f/2$ (direction of zero extension). $\phi_{peak} = \sin^{-1}[(\sigma_1 - \sigma_3)/(\sigma_1 + \sigma_3)]_{max}$ is the angle of internal friction, and $\nu_f = \sin^{-1}[-(d\epsilon_1 - d\epsilon_3)/(d\epsilon_1 + d\epsilon_3)]$ is the dilatancy angle at the peak state. In Fig. 4, most θ values are between θ_C and θ_R , and as a general trend, the angle θ decreases with D_{50}/W (as suggested by Vermeer, 1990). The θ_C value decreases also noticeably as σ_3 increases.

In Fig. 5(a), u_s^* at the start of residual state, $(u_s^*)_{res}$, is plotted against D_{50} . $(u_s^*)_{res}$ was defined as u_s^* at $R_n = 0.05$, and obtained by using the regression curve $R_n = \exp\{-\lambda(u_s^*/D_{50})^2\}$, where λ is a fitting parameter (Table 2). The data for Isomi gravel was omitted considering that the effects of membrane force would be too large, because of a large thickness (2.0 mm). Fig. 5(b) shows the relationships between "measured thickness of shear band t_0 " and D_{50} . t_0 (listed in Table 2) was defined as the distance between two parallel lines on which the rate of shear distortion along grid lines crossing the shear band was the maximum. It is seen from Figs. 5(a) and (b) that both $(u_s^*)_{res}$ and t_0 increase as D_{50} increases. An approximated value of $(u_s^*)_{res}$ for a given D_{50} can be estimated referring to the relations shown in Fig. 5(a). Then, when ϕ_{peak} , ϕ_{res} and $(u_s^*)_{res}$ are given, $R_n-u_s^*-u_n^*$ relations to be used in numerical analyses could be determined referring to the relations shown in Fig. 3.

As the effects of σ_3 were obvious, linear relations were obtained by regressing the data points separately for $\sigma_3 = 78$ or 392 kPa (see Figs. 5a and b). Scatters of plot from each regression curve are then due to other secondary factors, which may include crushability and shape of particles as discussed below.

The ratio $(u_s^*)_{res}/t_0$ is the average shear strain increment within the shear band which occurred between the peak state and the start of residual state. The value of $(u_s^*)_{res}/t_0$ ranges about 40 to 90 % for all tests (Fig. 5c), except for glass ballotini at $\sigma_3 = 392$ kPa. It may be seen that this ratio generally increases with D_{50} , but the trend is not clear.

4 PARTICLE CRUSHABILITY

To investigate the particle crushability of the test materials, a

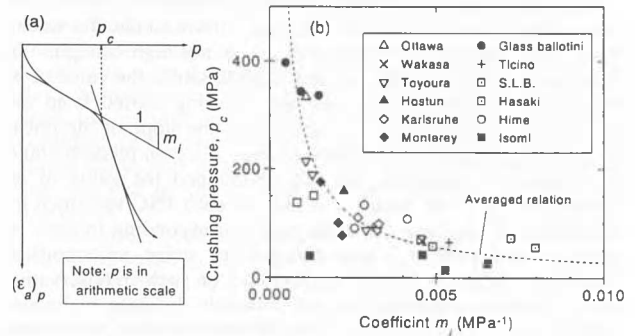


Figure 6. (a) Definition of p_c and m_i , (b) Observed p_c - m_i relation.

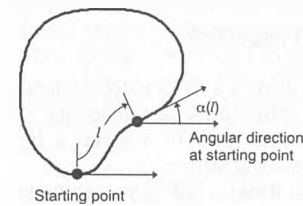


Figure 7. Angular function.

series of one-dimensional compression tests were performed. Both loose and dense specimens with a diameter of 4 cm and a height of 2.5 cm were compressed vertically up to 4.8, 9.8, 19.6, 39.2 or 73.5 MPa (50, 100, 200, 400 or 750 kgf/cm², respectively) at a constant axial strain rate of 0.2 %/min.

Fig. 6(a) illustrates a typical plastic axial strain $(\epsilon_a)_p$ and axial pressure p relation. Note that measured values of p include error due to friction at the inner surface of the container. $(\epsilon_a)_p$ was obtained by subtracting the elastic component $(\epsilon_a)_e$ from the measured total axial strain. $(\epsilon_a)_e$ was obtained from the response in many small unload/reload cycles with an amplitude of 4.9 MPa applied during each test.

As the pressure p exceeded some limit, particle crushing became intensive and the compressibility $d(\epsilon_a)_p/dp$ increased noticeably. This limit is called the crushing pressure (break point) p_c (e.g., Hagerty et al., 1993). In most of the tests where pressure p was applied up to $p_{max} = 73.5$ or 39.2 MPa, the value of p_c could be defined. The value of p_c indicates the crushability of particles: the higher p_c is, the less extent of crushing occurs. We also confirmed that intensive crushing of particles occurred when $p_{max} > p_c$ by sieving the specimen after unloading. p_c was defined as the pressure p at the crossing point of two tangents drawn at two linear portions of $(\epsilon_a)_p$ - p curve prior to and after the break point (Fig. 6a). The slope of the linear part below p_c (denoted by m_i) was also evaluated.

The values of void ratio e of the oedometer specimens were corrected by the method of Hardin (1985) for boundary errors due to small ratios of the specimen to particle sizes. The correction ranged from 0.005 (Ottawa sand) to 0.241 (Isomi

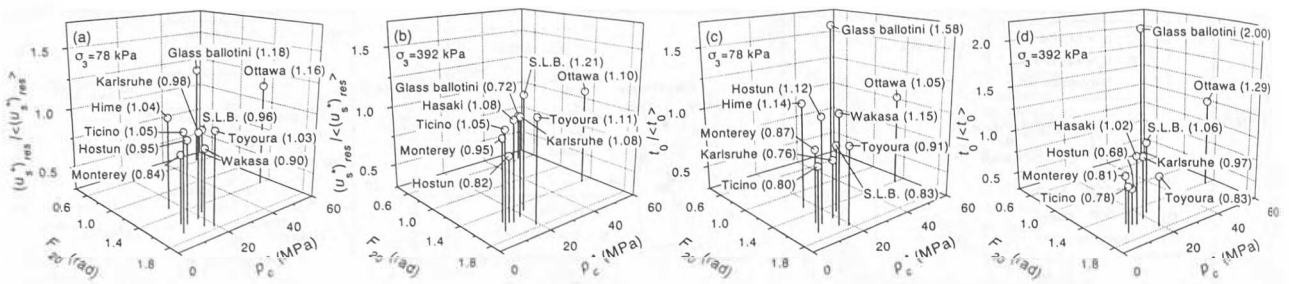


Figure 8. Influence of particle crushability and shape on $(u_s')_{res}$ and t_0 .

gravel). As p_c (and m_i also) is a function of void ratio e , the value corresponding to e of each PSC test was estimated.

For some tests, $e-p_c$ relation was not available. Namely, in tests using loose S.L.B., Karlsruhe and Ottawa sands, the values of p_c could not be defined since p_{max} was not high enough. In other tests using loose Hostun and Wakasa sands, the value of p_c could not be obtained since particle crushing started from the very initial loading stage (for these cases, the slope of the linear part of $(\epsilon_a)_p-p$ curve was defined as m_i). As $e-m_i$ relation could be obtained for all materials, we determined the value of m_i corresponding to the initial void ratio of each PSC specimen by interpolation, and then the value of p_c corresponding to each m_i value (denoted by p_c') was obtained by using an empirical relation $p_c = k/m_i$. This method is based on such an observation as that the p_c values for the test materials decrease in inverse proportion to m_i (Fig. 6b). The material constant k for each material was determined by least regression. We used p_c' as an index for particle crushability of each material.

5 PARTICLE SHAPE CHARACTERISTICS

We used plan views of particles taken by a CCD video camera to obtain the particle shape characteristics of the test materials. In the analysis, a micro-computer was used to achieve a high efficiency of analysis and avoid personal errors.

The angular function (Zahn and Roskies, 1972) was employed in the shape analysis. A starting point was selected arbitrarily on a closed curve defining the periphery of a particle. Then, along the periphery, total change in the angular direction α (in rad) accumulated from the starting point was obtained as a function of the arc length l from the starting point (Fig. 7). The function $\alpha(l)$ was transformed to a periodic function using the perimeter L as $\alpha_N(l) = \alpha(l) - 2\pi l/L$. $\alpha_N(l)$ was then expanded to a Fourier series as:

$$\alpha_N(x) = \frac{b_0}{2} + \sum_{k=1}^{\infty} \left(a_k \sin \frac{2\pi kl}{L} + b_k \cos \frac{2\pi kl}{L} \right) \quad (2)$$

The set of $\{a_k, b_k\}$ ($k \geq 1$) is independent of the position of the starting point and the perimeter L . The particle shape characteristics in terms of overall shape and local angularity are reflected in the coefficients of low and high orders, respectively. Using the truncated set of these coefficients, we defined an index for "the particle raggedness" F_{20} as:

$$F_{20} = \sum_{k=1}^{20} \sqrt{a_k^2 + b_k^2} \quad (3)$$

F_{20} has a dimension of the angle (in rad). F_{20} is zero for perfect spheres, and increases as the shape complexity increases. It was confirmed that F_{20} be well correlative with other representative indices e.g. "the total degree of angularity" (A_{2D}) (Lees, 1964). We used the value of F_{20} averaged for at least 20 particles sampled randomly as the representative value for each material.

6 RELATION BETWEEN DEFORMATION PROPERTY OF SHEAR BAND AND PARTICLE CHARACTERISTICS

To eliminate the effects of D_{50} and σ_3 , the ratio of the observed value of $(u_s')_{res}$ for each test to the value $\langle (u_s')_{res} \rangle$ predicted by the corresponding regression curve (for $\sigma_3 = 78$ or 392 kPa) shown in Fig. 5(a) was obtained. In Figs. 8(a) and (b), each ratio is plotted 3-dimensionally against on $p_c'-F_{20}$ plane. It may be noted that this ratio increases as p_c' increases, while the influence of F_{20} is not noticeable. The data of glass ballotini at $\sigma_3 = 392$ kPa is an exception, which is perhaps due to the very loose state of specimen (see Table 2).

Similarly, the ratio of the observed value of t_0 to the value $\langle t_0 \rangle$ predicted by the corresponding regression curve (for $\sigma_3 = 78$ or 392 kPa) shown in Fig. 5(b) is plotted in Figs. 8(c) and (d). Generally, this ratio increases as p_c' increases and as F_{20} decreases.

CONCLUSIONS

1. The angle of the direction of shear band relative to the σ_3 direction decreased with σ_3 and particle size.
2. Both "the shear deformation of shear band occurring between the peak state and the start of residual state $(u_s')_{res}$ " and "shear band thickness at the start of residual state t_0 " increased with D_{50} .
3. The average shear strain $(u_s')_{res}/t_0$ occurring between the peak state and the start of residual state ranged between about 40 % and 90 %.
4. The shear band thickness increased at the largest rate at the peak state.
5. Dilatation in shear band occurring between the peak state and the start of residual state increased with D_{50} .
6. Both $(u_s')_{res}$ and t_0 became smaller as σ_3 increased.
7. Both $(u_s')_{res}$ and t_0 became larger as the particle became less crushable.
8. t_0 became larger as the particle became rounder.

REFERENCES

- Goto, S., C.-S. Park, F. Tatsuoka and F. Molenkamp, 1993. Quality of the lubrication layer used in element tests on granular materials. *Soils and Foundations* 33-2: 47-59.
- Hagerty, M.M., D.R. Hite, C.R. Ullrich and D.J. Hagerty, 1993. One-dimensional high-pressure compression of granular media. *Journal of Geotechnical Engineering* 119-1: 1-18.
- Lees, G., 1964. A new method for determining the angularity of particles. *Sedimentology* 3: 2-21.
- Tatsuoka, F., T. Sato, C.-S. Park, Y.-S. Kim, J.N. Mukabi and Y. Kohata, 1994. Measuring of elastic properties of geomaterials in laboratory compression tests. *Geotechnical Testing Journal* 17-1: 80-94.
- Vermeer, P.A., 1990. The orientation of shear bands in biaxial tests. *Geotechnique* 40-2: 223-236.
- Yoshida, T., F. Tatsuoka, M.S.A. Siddiquee, Y. Kamegai and C.-S. Park, 1994. Shear banding in sands observed in plane strain compression. In R. Chambon, J. Desrues and I. Vardoulakis (eds), *Localisation and Bifurcation Theory for Soils and Rocks - Proc. 3rd Int. Workshop on Localisation and Bifurcation theory for Soils and Rocks*: 165-179. Balkema: Rotterdam.
- Zahn, C.T. and R.Z. Roskies, 1972. Fourier descriptors for plane closed curves. *IEEE Transactions on Computers* c-21-3: 269-281.